Research Article | Vol. 27, No. 24 / 25 November 2019 / Optics Express 34731

Optics EXPRESS

# Metal-graphene hybridized plasmon induced transparency in the terahertz frequencies

ANQI YU,[1,4] XUGUANG GUO,[1,4] YIMING ZHU,[1,*] ALEXEY V. BALAKIN,[1,2,3] AND ALEXANDER P. SHKURINOV[1,2,3]

[1] *Shanghai Key Lab of Modern Optical System, Terahertz Technology Innovation Research Institute, Terahertz Spectrum and Imaging Technology Cooperative Innovation Center, School of Optical- Electrical and Computer Engineering, University of Shanghai for Science and Technology, 516 Jungong Road, Shanghai 200093, China*

[2] *Department of Physics and International laser Center, Lomonosov Moscow State University, Leninskie Gory 1, Moscow 19991, Russia*

[3] *ILIT RAS – Branch of the FSRC "Crystallography and Photonics" RAS, Svyatoozerskaya 1, 140700, Shatura, Moscow Region, Russia*

[4] *These authors contributed equally*

[*] *ymzhu@usst.edu.cn*

**Abstract:** In this work, metal-graphene hybridized plasmon induced transparency (PIT) is systematically studied in the proposed simple metal/dielectric/graphene system. The PIT effect is the result of the coupling between the bright dipolar modes excited in the graphene regions under the shorter metallic bars and the dark quadrupolar modes excited in the graphene regions under the longer metallic bars. The coupled Lorentz oscillator model is used to help explain the physical origin of the PIT effect. Other than being tuned by the distance and the lateral displacement of the orthogonal metallic bars, the coupling efficiency can be further enhanced by the in-phase coupling or quenched by the out-of-phase coupling between the adjacent unit cells. Reduced barrier thickness will result in the enhancement of the coupling strengths and the scaling down of the device. Finally, we show that the PIT window can be actively tuned by changing the Fermi energy of graphene. The proposed structure has potential applications in actively tunable THz modulators, sensors and filters.



## 1. Introduction

In recent years, plasmon induced transparency (PIT) has attracted a lot of attention because of its potential applications in slow-light devices [1,2], chemical sensing [3,4], active plasmonic switches [5,6], waveguide modulators [7,8], band stop filters [9] and surface enhanced Raman scattering [10]. In analogy to electromagnetically induced transparency, PIT is a kind of interference effect that occurs in a three-level plasmonic metamaterial system. The PIT effect results from the interference between a bright (radiative) mode (which can be directly excited by the incident electromagnetic wave) and a dark (non-radiative) mode (which cannot be directly excited by the incident wave): the incident wave directly excites a bright mode, inducing a dip in the transmission spectrum and then the bright mode excites a dark mode by near field coupling, resulting in a transparency window within the dip. A dark mode is "dark" because it has 0 net dipole moment, such as a quadrupolar mode or a circular mode. In the past few years, PIT effect has been proposed and demonstrated by exciting quadrupolar modes in dolmen structures [11–15] and orthogonal bar structures [16], circular modes in split-ring resonators [17–20], non-concentric ring/disk arrays [21,22] and disk/disk arrays [5,10,23–25] both theoretically and experimentally in metallic structures.

Metallic surface-plasmons-based and spoof-surface-plasmons-based PIT effects, however, has little post-fabrication tunability. Consequently, the application of metallic PIT devices within a

#376100 https://doi.org/10.1364/OE.27.034731
Journal © 2019 Received 27 Aug 2019; revised 23 Oct 2019; accepted 23 Oct 2019; published 12 Nov 2019

Optics EXPRESS

broad frequency range requires multiple number of devices. PIT devices with post-fabrication tunability, on the other hand, can realize the PIT effect with much smaller number of devices, which is beneficial for integration. Recently researchers try to enhance the post-fabrication tunability of metal plasmons by the integration with liquid crystals [26–28]. Nevertheless, liquid crystals will introduce anisotropy in the dielectric environment and complicate the design of the structure. The direct contact of metal and graphene can also help to tune the metal-plasmon-caused PIT window within a short range by changing graphene Fermi energy [29,30]. Exciting plasmons in plasmonic materials whose plasmon dispersions are tunable by changing the carrier density is an alternate approach. PIT excited in patterned graphene, whose frequency can be actively tuned by changing the applied gate voltage, has recently been studied [31–36]. However, patterning graphene into certain structures will probably introduce contamination to graphene such as photoresist, which will degrade the quality of graphene [37]. The degradation in graphene mobility will weaken the PIT effect [33–35]. Therefore, it would be better to avoid further treatment to graphene such as photo-lithography in order to avoid such degradation of graphene. Xia et. al. proposed to realize graphene-plasmon-based PIT by using two graphene layers that are composed of an upper sinusoidally curved layer and a lower planar layer [38]. Realizing the PIT effect in a whole sheet of graphene with patterned metal is another alternative.

In this paper, the PIT effect is systematically studied in the proposed simple split T-shape metal/dielectric/graphene structure in the terahertz (THz) frequencies. Compared with traditional metal spoof-surface-plasmon-based PIT, the PIT effect in the proposed structure has post-fabrication tunability. Compared with patterned graphene structures, the graphene sheet will experience less quality-degrading processes. The split T-shape metal bars consist of longer horizontal and shorter vertical metallic bars, as shown in Fig. 1. The metallic bars are used to excite gated graphene plasmons. Unlike the quadrupolar mode formed by two out-of-phase dipolar modes in the dolmen structure, the gated quadrupolar mode under a single metallic bar is demonstrated to work as a dark mode. The dipolar mode excited in the graphene region gated by the shorter vertical bar functions as the bright mode. If the frequency of the dark quadrupolar mode is close to that of the bright dipolar mode and the two orthogonal metallic bars are close enough, PIT will be realized by the interaction between the bright mode and the dark mode. The PIT effect in the proposed structure can be excited either by center-excitation or edge-excitation. Therefore, other than being tuned by the distance and the lateral displacement between the orthogonal metallic bars, the coupling strength between the bright mode and the dark mode can be

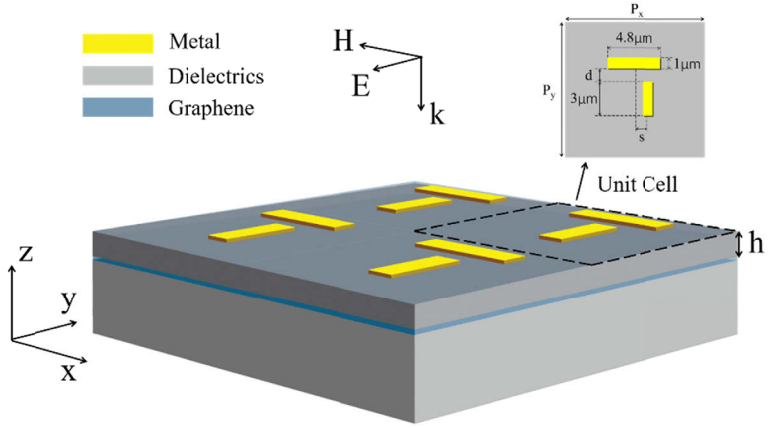


**Fig. 1.** (a) The proposed split T-shape metal/dielectric/graphene structure. (b) The top view of the proposed structure.

Optics EXPRESS

further enhanced by the in-phase interaction or quenched by the out-of-phase interaction between two adjacent T-shape structures when the metallic bars are rearranged. Since the gated graphene plasmons interact with the charges in metal, the enhancement of the coupling strengths and the scaling down of the device can be realized by simply reducing the spacing between graphene and the metallic bars. The transmission spectra of the structure are simulated by the finite difference time domain (FDTD) solutions and theoretically described by the coupled Lorentz oscillator model. The frequency of the PIT window can be actively tuned after fabrication by simply changing the Fermi energy of graphene. Such a feature indicates the potential applications such as active THz switch by changing the applied gate voltage of the proposed structure.

## 2. Simulation and model

The proposed structure is schematically shown in Fig. 1 and the top view of a unit cell is shown in the inset. The metallic structure in a unit cell consists of a shorter vertical one with length of 3μm and a longer horizontal one with length of 4.8μm. All metallic bars have the same thickness of 100nm and width of 1μm, and are modeled as perfect electric conductor (PEC). The distance between the horizontal and vertical bars is denoted by $d$. The lateral displacement between the central lines of the vertical and horizontal bars is denoted by $s$. If not specified, $d = 100$nm and $s = 0$nm. The metallic bars and graphene are separated by a thin dielectric barrier with initial thickness $h$ of 80nm. The refractive indices of the dielectric barrier and the substrate are 1.4. Generally, graphene should be modeled by the Kubo formula [29,33,35,38], which consists both the interband and the intraband contributions to the conductivity. However, in the THz frequencies the interband transition is forbidden according to the Pauli blocking, so that the interband contribution can be ignored and the intraband transition is the only contribution to the conductivity. Therefore, graphene is modeled by the Drude model instead of the Kubo formula with thickness of 1nm. The mobility $\mu$ of graphene is assumed to be 40,000cm$^2$/Vs and the scattering rate $\gamma$ is estimated by $1/\gamma = \mu E_F / e v_F{}^2$, with $E_F$ the graphene Fermi energy, $e$ the electron charge and $v_F = 10^8$cm/s the graphene Fermi velocity. If not specified, $E_F$=0.35eV. The horizontal and the vertical periods of a unit cell are initially set as $P_x$=6.1μm and $P_y$=6.2μm, respectively. The polarization of the incident radiation is along the y-axis.

To clarify the physical origin of the PIT effect, a coupled Lorentz oscillator model is adopted to analyze the transmission spectrum. The graphene region which is gated by the vertical bar is represented by oscillator 1 and the graphene region which is gated by the horizontal bar is represented by oscillator 2. As the charges $y_1(t)$ in oscillators 1 can be directly excited by the incident radiation and the charges $y_2(t)$ in oscillators 2 can only be driven by near field coupling with oscillator 1, they satisfy the following coupled equations [11,13,18–20,31–33]:

$$y_1''(t) + \gamma_1 y_1'(t) + \omega_1^2 y_1(t) + \kappa^2 y_2(t) = -\frac{e}{m}\beta_1^2 e^{-i\omega t} \tag{1}$$

$$y_2''(t) + \gamma_2 y_2'(t) + \omega_2^2 y_2(t) + \kappa^2 y_1(t) = 0 \tag{2}$$

where $\gamma_1$ and $\gamma_2$ are the dissipative damping constants in oscillators 1 and 2, respectively; $\omega_1$ and $\omega_2$ are the angular frequencies of the intrinsic resonance modes in oscillators 1 and 2, respectively; $\kappa$ is the coupling strength between the bright mode and the dark mode, ${\beta_1}^2$ is the coupling strength between the bright mode and the incident radiation, $m$ is the effective mass of graphene plasmons. Then the conductivity of oscillator 1 takes the form [39–43]:

$$\sigma_1(\omega) = \sigma_{Drude}(\omega) + \sigma_{PIT-1}(\omega) \tag{3}$$

$$\sigma_{Drude}(\omega) = i\sigma_0 \frac{4E_F}{\pi} \frac{1}{\hbar(\omega + i\gamma)} \tag{4}$$

Optics EXPRESS

$$\sigma_{PIT-1}(\omega) = i\sigma_0 \frac{4\beta_1^2 E_F \omega}{\pi\hbar} \frac{\omega^2 - \omega_2^2 + i\gamma_2\omega}{(\omega^2 - \omega_1^2 + i\gamma_1\omega)(\omega^2 - \omega_2^2 + i\gamma_2\omega) - \kappa^4} \tag{5}$$

where $\sigma_0$=$e^2/4\hbar$ is the universal conductivity of graphene, $\hbar$ is the reduced Plank constant, $\sigma_{Drude}$ is the Drude background conductivity and $\sigma_{PIT-1}$ is the conductivity of the 1st coupled bright-dark mode. (Here the conductivities of the higher order modes are not taken into account because they are out of our consideration.) The transfer matrix of the graphene layer is [43,44]

$$G = \begin{pmatrix} \frac{n_1+n_2+\frac{\sigma_1(\omega)}{c\varepsilon_0}}{2n_1} & \frac{n_1-n_2+\frac{\sigma_1(\omega)}{c\varepsilon_0}}{2n_1} \\ \frac{n_1-n_2-\frac{\sigma_1(\omega)}{c\varepsilon_0}}{2n_1} & \frac{n_1+n_2-\frac{\sigma_1(\omega)}{c\varepsilon_0}}{2n_1} \end{pmatrix} \tag{6}$$

where $c$ is the speed of light in vacuum, $\varepsilon_0$ is the vacuum permittivity, $n_1$=1 is the refractive index of air and $n_2$=1.4 is the refractive index of the substrate. Then the relationship of the incidence, the reflectance and the transmission can be given as

$$\begin{pmatrix} E_{inc} \\ E_{ref} \end{pmatrix} = G \cdot \begin{pmatrix} E_{tran} \\ 0 \end{pmatrix} \tag{7}$$

where $E_{inc}$, $E_{ref}$ and $E_{tran}$ represent the incidence, the reflectance and the transmission, respectively. The transmission spectrum is calculated as

$$T(\omega) = \left| \frac{E_{tran}}{E_{inc}} \right|^2 \cdot n_2 \tag{8}$$

## 3. Results and discussion

The simulated transmission spectrum of the proposed structure when illuminated by normally incident y-polarized THz waves is shown in Fig. 2(a) by the red curve. It can be seen that there are two dips at 3.54THz (denoted by A) and 4.03THz (denoted by C) with a transparency window peaked at 3.83THz (denoted by B) and the PIT effect is realized. The transmission spectrum calculated by the coupled oscillator model is also shown in Fig. 2(a) by the red circles. The simulated transmission spectrum of the vertical-bar structure and the horizontal-bar structure are also shown in Fig. 2(a) by the black and the blue curves, respectively. The transmission spectrum of the vertical-bar and horizontal-bar structures are calculated by the single oscillator model (by setting $\kappa$ in the coupled oscillator model as 0), as shown in Fig. 2(a) by the black squares and blue triangles, respectively. It is seen that the vertical-bar structure shows a transmission dip at 3.81THz while the horizontal-bar structure shows no peaks or dips within the concerned frequency range. The $Re(E_z)$ distributions of the vertical-bar-only structures at 3.81THz is plotted in Fig. 2(b). It is obvious that the dip is caused by the dipolar mode excited in the gated graphene region under the vertical bar. The $Re(E_z)$ distribution of dip A, peak B and dip C are shown in Fig. 2(c). Apparently, the graphene region under the vertical bar shows dipolar resonance for dips A and C, which means that the excited dipolar mode leads to transmission dips. For peak B, however, the dipolar mode is greatly suppressed and the graphene region under the horizontal bar shows strong quadrupolar resonance.

The PIT effect is known to result from the interaction between a bright mode and a dark mode [5–7,10–16,18–24,29,30,36,38] or the interaction between two bright modes [9,45,46]. According to the electric field distributions given in Fig. 2, the dipolar mode works as a bright mode and the quadrupolar mode functions as a dark mode. The PIT effect in the proposed structure results from the coupling between the bright dipolar mode and the dark quadrupolar mode. The correspondence between the calculated and simulated spectra also suggests that the

Optics EXPRESS

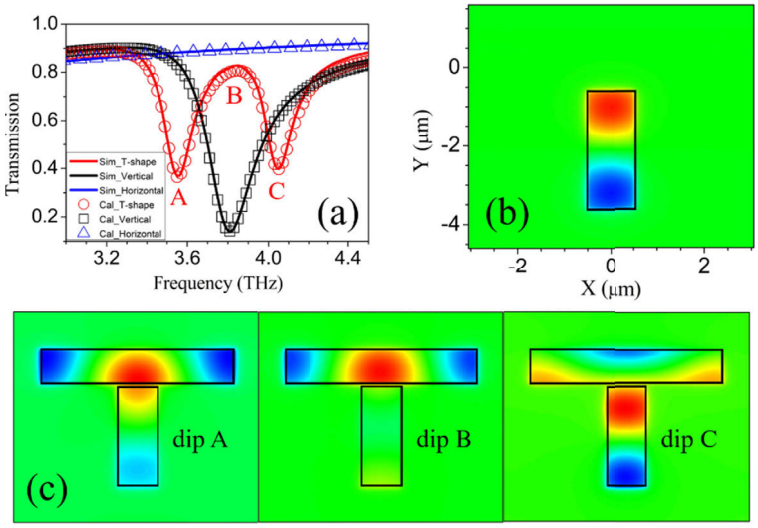


**Fig. 2.** (a) The simulated transmission spectra (solid curves) of the proposed spilt T-shape structure (red), vertical-bar structure (black) and horizontal-bar structure (blue) and the calculated transmission spectra of the proposed spilt T-shape structure (red circles), vertical-bar structure (black squares) and horizontal-bar structure (blue triangles). (b) The $Re(E_z)$ distributions of the vertical-bar-only structure. (c) The $Re(E_z)$ distributions of dip A, peak B and dip C.

PIT effect in this work is the result of the coupling of a bright mode and a dark mode. A detailed explanation is given as follows. When the y-polarized THz wave is incident upon the proposed structure, it will directly excite the bright dipolar mode, known as the excitation pathway $|0> \rightarrow |1>$. When the bright dipolar mode is excited, it will interact with the dark quadrupolar mode $|2>$ of the gated graphene under the longer horizontal metallic bar by near field coupling. Then there will be another excitation pathway of the bright mode $|0> \rightarrow |1> \rightarrow |2> \rightarrow |1>$. The two excitation pathways destructively interact with each other so that the excitation efficiency of the bright mode is reduced, opening a transparency window in the transmission dip of the bright mode.

As the interaction between the bright mode and the dark mode relies on near field coupling, the coupling efficiency should rely on the distance between the bright mode and the dark mode. That is, the smaller the distance between the horizontal bar and the vertical bar is, the stronger the near field coupling is, and then the deeper and wider the transparency window is. To further verify that the transparency window shown in Fig. 2(a) is the result of the coupling between the dark quadrupolar mode and the bright dipolar mode, the distance $d$ between the horizontal and vertical bars is gradually increased from 200nm to 1600nm. $P_y$ is set as 10μm to avoid the interaction between the vertical bar and the horizontal bar in the lower adjacent unit cell. The simulated transmission spectra as shown in Fig. 3(a) show that the transparency peak becomes weaker and weaker as $d$ increases, which is consistent with the reducing coupling strength $\kappa$ as shown in Fig. 3(b). The simulated $|E_z|$ distributions as shown in Fig. 3(c) show that the bright dipolar mode gets stronger and stronger as $d$ increases. Thus, both simulation and calculation results indicate that the coupling strength between the bright dipolar and dark quadrupolar modes is reduced with the increase of $d$ and the transparency window is the result of the coupling between the bright and dark modes.

The coupling between the bright and dark modes can be tuned not only by $d$ but also by lateral displacement $s$. The transmission spectra as shown in Fig. 4(b) show that the transparency peak

Optics EXPRESS

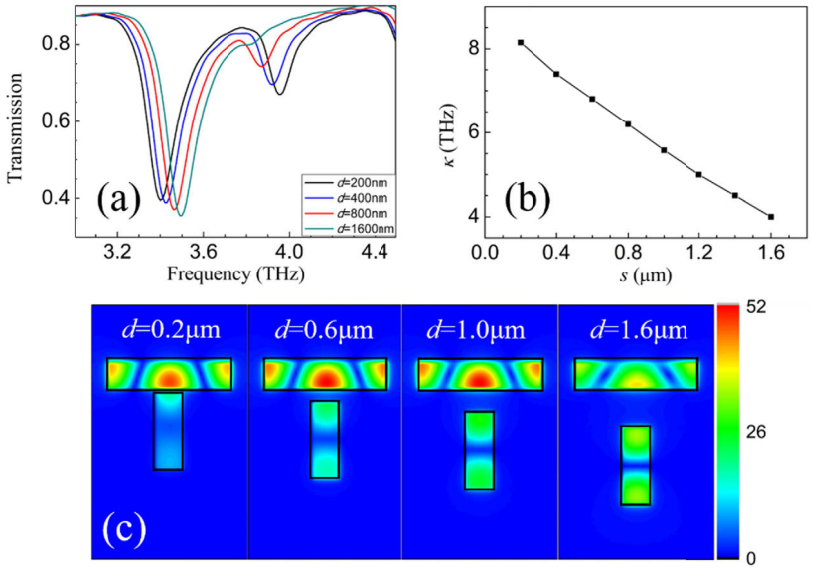


**Fig. 3.** (a) The simulated transmission spectra of the proposed spilt T-shape structure with $P_y$=10μm and $d$ changing from 200nm to 1600nm. (b) The coupling strengths $\kappa$ with $d$ changing from 200nm to 1600nm with a step of 200nm. (c) The $|E_z|$ distributions with $d$ = 200nm, 600nm, 1000nm and 1600nm.

becomes weaker and weaker with the increase of $s$ and disappears when $s$ = 1.5μm ($P_x$ is set as 10μm to avoid the coupling between the vertical bar and the horizontal bar in the right unit cell). After that, the transparency peak emerges again. Accordingly, the $Re(E_z)$ distributions are given in Fig. 4(c) and the change in the coupling strength $\kappa$ as a function of $s$ is plotted in Fig. 4(d). It can be seen from the $Re(E_z)$ distributions that the electric field under the horizontal bar is always nearly symmetric. Because of the symmetry, the coupling between the bright mode and the dark mode is strongest when the end of the vertical bar is against a "node region", that is, $s$≈0μm or $s$≈2.4μm; when the vertical bar is against an "anti-node region", that is, $s$≈1.5μm, the coupling is extremely weak.

The translation of the vertical bar shows that the dark quadrupolar mode can be efficiently excited by the bright dipolar mode through both middle- and side-excitations. Therefore, $\kappa$ can be strengthened if the split-T shape bar sets are rearranged from rectangular-like to rhombus-like by periodically translating some of the split-T shape bars in the y-direction as shown in Fig. 5(a). Once the rearrangement is done, $P_x$=6.1μm automatically doubles. The transmission spectra with the decrease in $P_x$ is shown in Fig. 5(b). Obviously, the transparency window becomes wider and wider, indicating the strengthening of $\kappa$. The change in $\kappa$ as shown in Fig. 5(c) directly shows the enhancement of $\kappa$. The $Re(E_z)$ distribution given in Fig. 5(d) shows that the charges in both coupling regions as denoted by the pink circles show opposite signs. Thus, the dark mode excited by the bright mode in the same unit cell and the dark mode excited by the bright mode in the adjacent unit cell (denoted by the pink dashed ellipse in Fig. 5(d)) are in phase, resulting in the enhancement of the coupling between the bright mode and the dark mode. On the contrary, if the translated split T-shape bars are rotated around the red point R by 180 degrees as shown in Fig. 6(a), the dark mode excited by the bright mode in the same unit cell and the dark mode excited by the bright mode in the adjacent unit cell are out of phase. Then, the excitation of the dark mode will be suppressed and the transparency window will become narrower and narrower when $P_x$ decreases as shown in Fig. 6(b). In this case, the coupling strength $\kappa$ monotonously

Optics EXPRESS

decreases with the decrease in $P_x$ as shown in Fig. 6(c). When $P_x \leq 6.6\mu m$, the transparency window nearly completely vanishes because the dark quadrupolar mode is nearly completely suppressed, as shown by the $|E_z|$ distribution in Fig. 6(d).

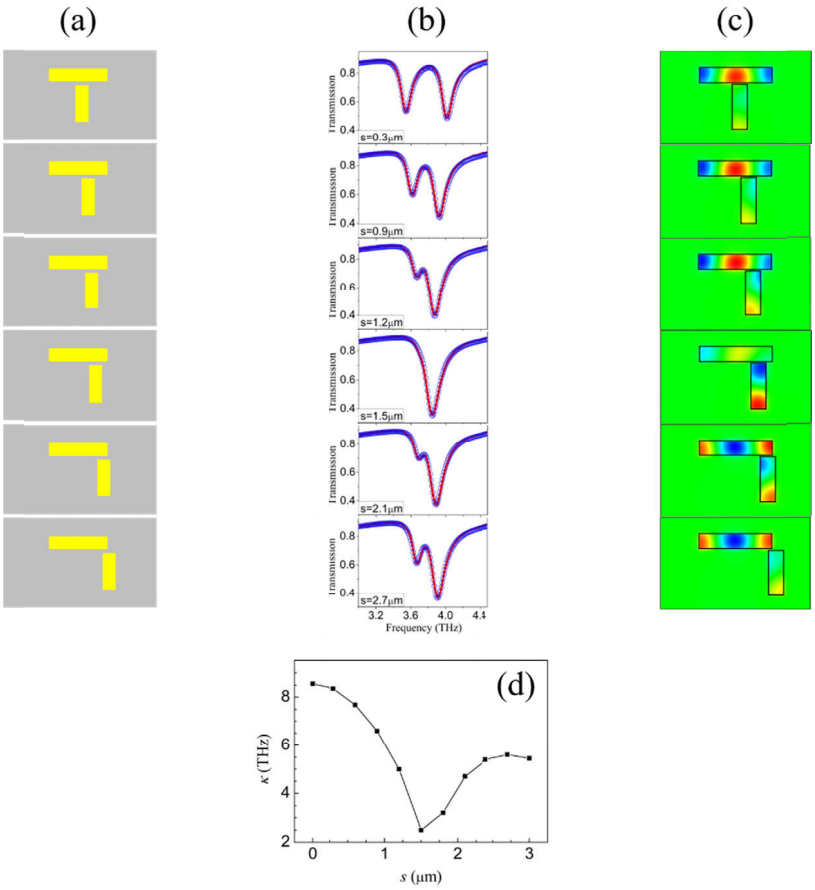


**Fig. 4.** (a) The schematics of the change in $s$ with $P_x$=10μm and $s$ increased from 0.3μm to 2.7μm. (b) The simulated transmission spectra (red solid curves) and the calculated transmission spectra (blue circles) corresponding to the structures shown in (a). (c) $Re(E_z)$ distributions of the structures shown in (a). (d) The change in the coupling strength $\kappa$ as a function of $s$.

Once closely gated by metal, graphene or semiconductor plasmons will attractively interact with the charges in metal and their dispersions will change from a quadratic one to a linear-like one with $\omega \propto \sqrt{h}$ [47–49]. As the gated graphene plasmons are excited by metal, the thickness $h$ of the dielectric barrier which separates graphene and the metal bars will influence the frequency of the PIT window. The transmission spectra as a function of $h$ is shown in Fig. 7(a). It can be seen that the frequency of the PIT window shows clear blueshift as $h$ increases. As a result of the weakened metal-graphene interaction, both ${\beta_1}^2$ and the relative coupling strength $\kappa/\omega_2$ decreases with increasing $h$ as shown in Fig. 7(b). Then it can be inferred that both the enhancement of coupling strength and the scaling down of the device can be achieved by decreasing $h$.

Finally, we show that the frequency of the transparency window can be tuned by the Fermi energy of graphene because the dispersion of graphene plasmons is influenced by the Fermi energy. As shown in Fig. 8, the center of the transparency window can be tuned from 2.89THz when $E_F$=0.2eV to 6.16THz when $E_F$=0.9eV. The transmission at the resonance dips becomes

Optics EXPRESS

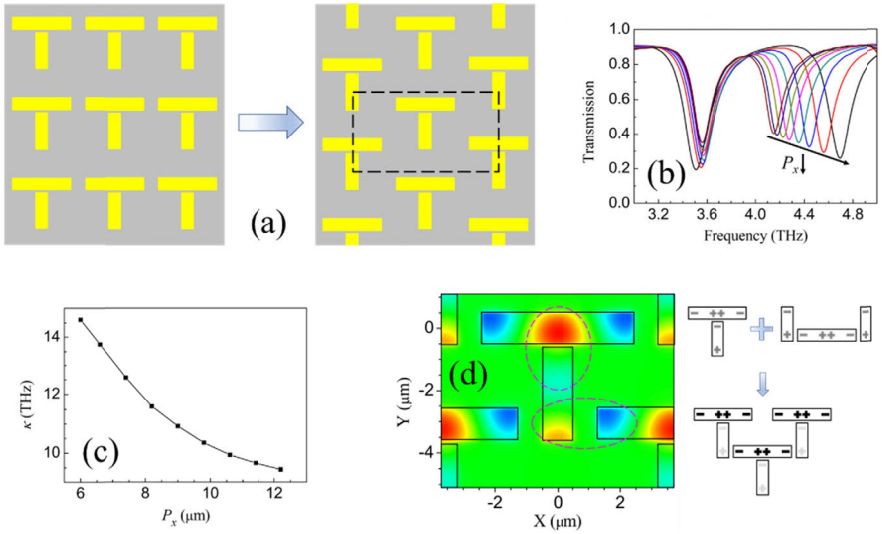


**Fig. 5.** (a) The rearrangement of the split T-shape structure. (b) The simulated transmission spectra of the rearranged spilt T-shape structure with $P_x$ reduced from 12.2μm to 6μm. (c) The coupling strengths $\kappa$ corresponding to the spectra shown in (a). (d) The $Re(E_z)$ distribution with $P_x = 7.4$μm. The inset indicates the in-phase coupling between the adjacent split-T shape structures.

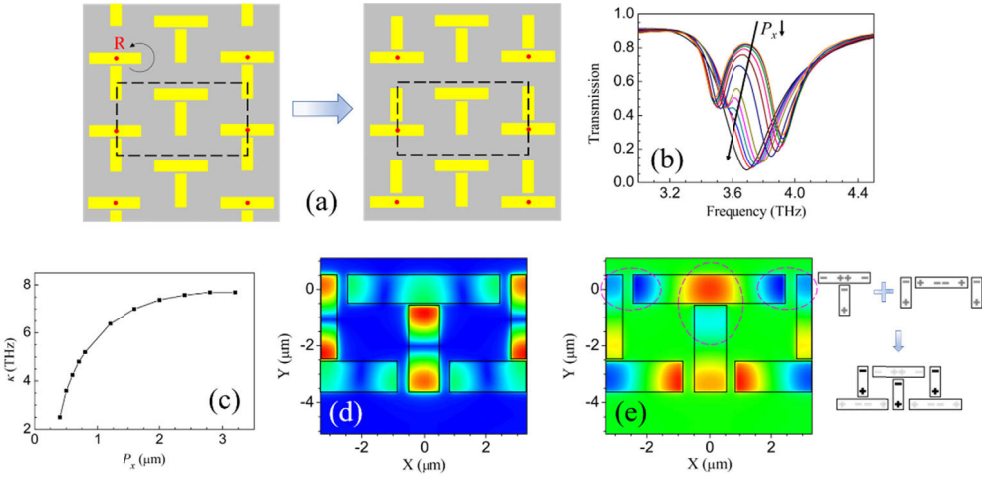


**Fig. 6.** (a) The schematics of rotating the translated split T-shape bars by 180 degrees around the point R. The dashed rectangles indicate a unit cell. (b) The simulated transmission spectra of the rearranged spilt T-shape structure with $P_x$ reduced from 12.2μm to 6μm. (c) The coupling strengths $\kappa$ corresponding to the spectra shown in (a). (d) The $|E_z|$ distribution with $P_x$=6.6μm. (e) The $Re(E_z)$ distribution with $P_x$=6.6μm. The inset indicates the out-of-phase coupling between the adjacent split-T shape structures.

Optics EXPRESS

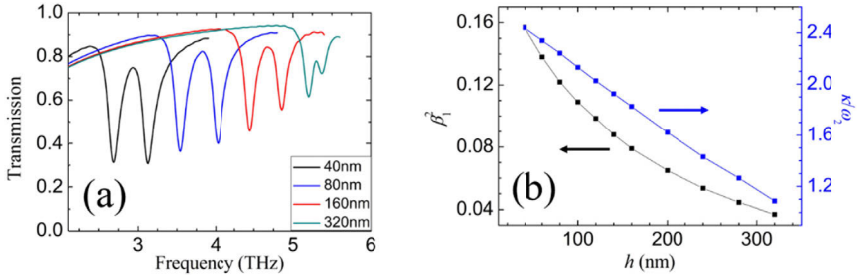


**Fig. 7.** (a) The transmission spectra with $h = 40$nm (black), 80nm (blue), 160nm (red) and 320nm (dark cyan). (b) The change in ${\beta_1}^2$ and $\kappa/\omega_2$ as a function of $h$.

lower while the transmission at the transparency window becomes higher because of the reduction in $\gamma$. Therefore, both the frequency and the peak-to-dip ratio can be changed by tuning up the Fermi energy of graphene.

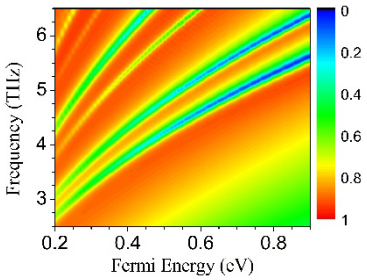


**Fig. 8.** The contour of the transmission spectra by increasing the Fermi energy of graphene from 0.2eV to 0.9eV.

## 4. Conclusions

In conclusion, we propose to realize the PIT effect in split T-shape metal/dielectric/graphene structure. The PIT effect results from the coupling between the bright dipolar mode excited in the graphene region under the vertical metallic bar and the dark quadrupolar mode excited in the graphene region under the horizontal metallic bar. The coupling strength between the bright mode and the dark mode can be tuned by the distance $d$ between the vertical and horizontal bars, the lateral displacement $s$ between the central lines of the vertical and horizontal bars. Rearranging the split T-shape metallic bars from rectangle-like to rhombus-like, the coupling strength can be greatly enhanced with the reduction in $P_x$ because the dark mode excited by the bright mode in the same unit cell and the dark mode excited by the bright mode in the adjacent unit cell are in phase. By rotating the split T-shape bars in the rearranged structure around the R point by 180 degrees, the coupling strength will be weakened with the reduction in $P_x$ because the dark mode excited by the bright mode in the same unit cell and the dark mode excited by the bright mode in the adjacent unit cell are out of phase. The reduction in $h$ will lead to the strengthening of the coupling strengths as a result of enhanced graphene-metal interaction. Finally, it is shown that the frequency and the peak-to-dip ratio are both tunable by the Fermi energy of graphene. The results may find applications in slow-light devices, sensing, active plasmonic switches and active band stop filters.

Optics EXPRESS

## Funding

National Key Research and Development Program of China (2017YFA0701005); National Natural Science Foundation of China (61722111); International Joint Lab Program supported by Science and Technology Commission Shanghai Municipality (17590750300); Overseas Expertise Introduction Project for Discipline Innovation (D18014).

## References

1. T. F. Krauss, "Why do we need slow light?" Nat. Photonics **2**(8), 448–450 (2008).
2. C. Wu, A. B. Khanikaev, and G. Shvets, "Broadband Slow Light Metamaterial Based on a Double-Continuum Fano Resonance," Phys. Rev. Lett. **106**(10), 107403 (2011).
3. J. F. O'Hara, R. Singh, I. Brener, E. Smirnova, J. Han, A. J. Taylor, and W. Zhang, "Thin-film sensing with planar terahertz metamaterials: sensitivity and limitations," Opt. Express **16**(3), 1786–1795 (2008).
4. X. He, Q. Zhang, G. Lu, G. Ying, F. Wu, and J. Jiang, "Tunable ultrasensitive terahertz sensor based on complementary graphene metamaterials," RSC Adv. **6**(57), 52212–52218 (2016).
5. W.-S. Chang, J. B. Lassiter, P. Swanglap, H. Sobhani, S. Khatua, P. Nordlander, N. J. Halas, and S. Link, "A Plasmonic Fano Swith," Nano Lett. **12**(9), 4977–4982 (2012).
6. M. Amin, R. Ramzan, and O. Siddiqui, "Fano resonance based ultra high-contrast electromagnetic switch," Appl. Phys. Lett. **110**(18), 181904 (2017).
7. X. Piao, S. Yu, and N. Park, "Control of Fano asymmetry in plasmon induced transparency and its application to plasmonic waveguide modulator," Opt. Express **20**(17), 18994–18999 (2012).
8. Z. Chai, X. Hu, H. Yang, and Q. Gong, "All-optical tunable on-chip plasmon-induced transparency based on two surface-plasmon-polaritons absorption," Appl. Phys. Lett. **108**(15), 151104 (2016).
9. Y. Liu, R. Zhong, Z. Lian, C. Bu, and S. Liu, "Dynamically tunable band stop filter enabled by the metal-graphene metamaterials," Sci. Rep. **8**(1), 2828 (2018).
10. J. Ye, F. Wen, H. Sobhani, J. B. Lassiter, P. V. Dorpe, P. Nordlander, and N. J. Halas, "Plasmonic nanoclusters: near field properties of the Fano resonance interrogated with SERS," Nano Lett. **12**(3), 1660–1667 (2012).
11. S. Zhang, D. A. Genov, Y. Wang, M. Liu, and X. Zhang, "Plasmon-induced transparency in metamaterials," Phys. Rev. Lett. **101**(4), 047401 (2008).
12. N. Liu, M. Hentschel, T. Weiss, A. P. Alivisatos, and H. Giessen, "Three-dimensional plasmon rulers," Science **332**(6036), 1407–1410 (2011).
13. N. Liu, L. Langguth, T. Weiss, J. Kästel, M. Fleischhauer, T. Pfau, and H. Giessen, "Plasmonic analogue of electromagnetically induced transparency at the Drude damping limit," Nat. Mater. **8**(9), 758–762 (2009).
14. N. K. Emani, T. Fung Chung, A. V. Kildishev, V. M. Shalaev, Y. P. Chen, and A. Boltasseva, "Electrical modulation of Fano resonance in plasmonic nanostructures using graphene," Nano Lett. **14**(1), 78–82 (2014).
15. A. Halpin, C. Mennes, A. Bhattacharya, and J. G. Rivas, "Visualizing near-field coupling in terahertz dolmens," Appl. Phys. Lett. **110**(10), 101105 (2017).
16. M. Miyata, J. Hirohata, Y. Nagasaki, and J. Takahara, "Multi-spectral plasmon induced transparency via in-phane dipole and dual quadrupole coupling," Opt. Express **22**(10), 11399–11406 (2014).
17. V. A. Fedotov, M. Rose, S. L. Prosvirnin, N. Papasimakis, and N. I. Zheludev, "Sharp trapped-mode resonances in planar metamaterials with a broken structural symmetry," Phys. Rev. Lett. **99**(14), 147401 (2007).
18. J. Gu, R. Singh, X. Liu, X. Zhang, Y. Ma, S. Zhang, S. A. Maier, Z. Tian, A. K. Azad, H.-T. Chen, A. J. Taylor, J. Han, and W. Zhang, "Active control of electromagnetically induced transparency analogue in terahertz metamaterials," Nat. Commun. **3**(1), 1151 (2012).
19. S. Li, P. S. Nugraha, X. Su, X. Chen, Q. Yang, M. Unferdorben, F. Kovács, S. K. Máté, M. Liu, X. Zhang, C. Ouyang, Y. Li, J. A. Fülöp, J. Han, and W. Zhang, "Terahertz electric field modulated mode coupling in graphene-metal hybrid metamaterials," Opt. Express **27**(3), 2317–2326 (2019).
20. J. Ji, S. Zhou, W. Wang, C. Luo, Y. Liu, Y. Liu, F. Ling, and J. Yao, "Active multifunctional terahertz modulator based on plasmonic metasurface," Opt. Express **27**(3), 2363–2373 (2019).
21. Y. Sonnefraud, N. Verellen, H. Sobhani, G. A. E. Vandenbosch, V. V. Moshchalkov, P. V. Dorpe, P. Nordlander, and S. A. Maier, "Experimental realization of subradiant, superradiant, and Fano resonances in ring/disk plasmonic nanocavities," ACS Nano **4**(3), 1664–1670 (2010).
22. F. Hao, P. Nordlander, Y. Sonnerfraud, P. V. Dorpe, and S. A. Maier, "Tunability of subradiant dipolar and Fano-type plasmon resonances in metallic ring/disk cavities: implications for nanoscale optical sensing," ACS Nano **3**(3), 643–652 (2009).
23. D. Dregely, M. Hentschel, and H. Giessen, "Excitation and tuning of higher-order Fano resonances in plasmonic oligomer clusters," ACS Nano **5**(10), 8202–8211 (2011).
24. F. Wen, J. Ye, N. Liu, P. V. Dorpe, P. Nordlander, and N. J. Halas, "Plasmon Transmutation: Inducing new modes in nanoclusters by adding dielectric nanoparticles," Nano Lett. **12**(9), 5020–5026 (2012).
25. J. B. Lassiter, H. Sobhani, M. W. Knight, W. S. Mielczarek, P. Nordlander, and N. J. Halas, "Designing and deconstructing the Fano linshape in plasmonic nanoclusters," Nano Lett. **12**(2), 1058–1062 (2012).

Optics EXPRESS


26. D. Franklin, R. Frank, S.-T. Wu, and D. Chanda, "Actively addressed single pixel full-color plasmonic display," Nat. Commun. **8**(1), 15209 (2017).
27. R. Bartholomew, C. Williams, A. Khan, R. Bowman, and T. Wilkinson, "Plasmonic nanohole electrodes for active color tunable liquid crystal transmissive pixels," Opt. Lett. **42**(14), 2810–2813 (2017).
28. R. Wang, L. Li, J. Liu, F. Yan, F. Tian, H. Tian, J. Zhang, and W. Sun, "Triple-band tunable perfect terahertz metamaterial absorber with liquid crystal," Opt. Express **25**(26), 32280–32289 (2017).
29. C. Sun, Z. Dong, J. Si, and X. Deng, "Independently tunable dual-band plasmonically induced transparency based on hybrid metal-graphene metamaterials at mid-infrared frequencies," Opt. Express **25**(2), 1242–1250 (2017).
30. J. Chen, X. Li, X. Shi, C. Fan, M. Tuhtasu, X. He, W. Shi, and F. Liu, "Active control of light slowing enabled bu coupling electromagnetic metamaterials with low-lossy graphene," Opt. Lett. **43**(20), 4891–4894 (2018).
31. W. Tang, L. Wang, X. Chen, C. Liu, A. Yu, and W. Lu, "Dynamic metamaterial based on the graphene split ring high-Q Fano-resonator for sensing applications," Nanoscale **8**(33), 15196–15204 (2016).
32. H. Cheng, S. Chen, P. Yu, X. Duan, B. Xie, and J. Tian, "Dynamically tunable plasmonically induced transparency in periodically patterned graphene nanostrips," Appl. Phys. Lett. **103**(20), 203112 (2013).
33. X. Zhao, C. Yuan, L. Zhu, and J. Yao, "Graphene-based tunable terahertz plasmon-induced transparency metamaterial," Nanoscale **8**(33), 15273–15280 (2016).
34. X. He, Y. Huang, X. Yang, L. Zhu, F. Wu, and J. Jiang, "Tunable electromagnetically induced transparency based on terahertz graphene metamaterial," RSC Adv. **7**(64), 40321–40326 (2017).
35. M. Cao, T. Wang, H. Zhang, and Y. Zhang, "Tunable electromagnetically induced absorption based on graphene," Opt. Commun. **413**, 73–79 (2018).
36. S.-X. Xia, X. Zhai, L.-L. Wang, and S.-C. Wen, "Plasmonically induced transparency in double-layered graphene nanoribbons," Photonics Res. **6**(7), 692–702 (2018).
37. B. H. Son, H. S. Kim, H. Jeong, J.-Y. Park, S. Lee, and Y. H. Ahn, "Electron beam induced removal of PMMA layer used for graphene transfer," Sci. Rep. **7**(1), 18058 (2017).
38. S.-X. Xia, X. Zhai, L.-L. Wang, B. Sun, J.-Q. Liu, and S.-C. Wen, "Dynamically tunable plasmonically induced transparency in sinusoidally curved and planar graphene layers," Opt. Express **24**(16), 17886–17899 (2016).
39. V. V. Popov, D. V. Fateev, O. V. Polischuk, and M. S. Shur, "Enhanced electromagnetic coupling between terahertz radiation and plasmons in a grating-gate transistor structure on membrane substrate," Opt. Express **18**(16), 16771–16776 (2010).
40. C. S. R. Kaipa, A. B. Yakovlev, G. W. Hanson, Y. R. Padooru, F. Medina, and F. Mesa, "Enhanced transmission with a graphene-dielectric microstructure at low-terahertz frequencies," Phys. Rev. B **85**(24), 245407 (2012).
41. I. V. Iorsh, I. S. Mukhin, I. V. Shadrivov, P. A. Belov, and Y. S. Kivshar, "Hyperbolic metamaterials based on multilayer graphene structures," Phys. Rev. B **87**(7), 075416 (2013).
42. C. H. Gan, H. S. Chu, and E. P. Li, "Synthesis of highly confined surface plasmon modes with doped graphene sheets in the midinfrared and terahertz frequencies," Phys. Rev. B **85**(12), 125431 (2012).
43. N. M. R. Peres and Y. V. Bludov, "Enhancing the absorption of graphene in the terahertz range," EPL **101**(5), 58002 (2013).
44. T. Zhan, X. Shi, Y. Dai, X. Liu, and J. Zi, "Transfer matrix method for optics in graphene layers," J. Phys.: Condens. Matter **25**(21), 215301 (2013).
45. C.-Y. Chen, I.-W. Un, N.-H. Tai, and T.-J. Yen, "Asymmetric coupling between subradiant and superradiant plasmonic resonances and its enhanced sensing performance," Opt. Express **17**(17), 15372–15380 (2009).
46. X.-R. Jin, J. Park, H. Zheng, S. Lee, Y. Lee, J. Y. Rhee, K. W. Kim, H. S. Cheong, and W. H. Jang, "Highly-dispersive transparency at optical frequencies in planar metamaterials based on two-bright-mode coupling," Opt. Express **19**(22), 21652–21657 (2011).
47. A. Eguiluz, T. K. Lee, J. J. Quinn, and K. W. Chiu, "Interface excitations in metal-insulator-semiconductor structures," Phys. Rev. B **11**(12), 4989–4993 (1975).
48. D. V. Fateev, V. V. Popov, and M. S. Shur, "Transformation of the plasmon spectrum in a grating-gate transistor structure with spatially modulated two-dimensional electron channel," Semiconductors **44**(11), 1406–1413 (2010).
49. L. Wang, W. Hu, J. Wang, X. Wang, S. Wang, X. Chen, and W. Lu, "Plasmon resonant excitation in grating-gated AlN barrier transistors at terahertz frequency," Appl. Phys. Lett. **100**(12), 123501 (2012).